A core/shell mechanism for stacking-fault generation in GaAs nanowires

Zaoshi Yuan, Ken-ichi Nomura, and Aiichiro Nakano
Collaboratory for Advanced Computing and Simulations, Department of Physics and Astronomy, Department of Computer Science, Department of Chemical Engineering and Materials Science, University of Southern California, Los Angeles, California 90089-0242, USA

(Received 16 December 2011; accepted 27 March 2012; published online 16 April 2012)

Generation of stacking faults (SFs) during the growth of nanowires (NWs) is a major concern for the efficiency of NW-based devices such as solar cells. Here, molecular-dynamics simulation of a [111]-oriented gallium arsenide NW reveals an atomistic mechanism of SF generation. Spatial distribution of the adatom energy on the (111)B top surface exhibits a core/shell structure due to the contraction of atomic bonds at the sidewall surfaces, where SFs are preferentially nucleated in the shell. A nucleation growth model incorporating the core/shell mechanism suggests a size and growth-condition controlled approach for SF-free growth of NWs. © *2012 American Institute of Physics*. [http://dx.doi.org/10.1063/1.3703765]

Nanowires (NWs) composed of semiconductor such as gallium arsenide (GaAs) have broad applications including solar cells[1] due to their unique physical properties at the nanometer scale.[2–4] GaAs NWs have traditionally been grown by the vapor-liquid-solid (VLS) technique.[5] Recently, an alternative growth method called selective area metal organic vapor-phase epitaxy (SA-MOVPE) has attracted much attention due to its ability to form atomically sharp interfaces to fabricate axial heterostructures such as tandem NW solar cells.[6] The catalyst-free SA-MOVPE method also avoids metal impurities that degrade NW performance.[6] However, a major problem of non-VLS-grown NWs is a large number of stacking faults (SFs) that may alter electronic properties and degrade device performance.[6,7] In the case of VLS growth, previous works have pointed out the importance of the edge of the NW top surface in dictating the grown crystalline phase.[8] Though semi-empirical explanations based on surface energies have been attempted,[8] atomistic mechanisms underlying the edge-mediated SF nucleation remain elusive, especially for SA-MOVPE.

Here, molecular-dynamics (MD) simulation reveals a core/shell structure for adatom energetics on the (111)B top surface of a [111]-oriented GaAs NW, in which SFs are preferentially nucleated in the shell. A nucleation growth model suggests optimal growth temperature and pressures for minimizing SFs as well as a size-controlled growth method for eliminating them.

We perform MD simulation of a GaAs NW with diameter $D_w \sim 30$ Å.[9] The NW axis is the [111] orientation of zinc-blende (ZB) crystal, and the hexagonal NW has six $\{1\bar{1}0\}$ sidewalls (see Fig. 1(a)). The interatomic potential used in the MD simulation has been validated against various experimental and quantum-mechanical (QM) results.[10] In particular, the interatomic potential reproduces the contraction of Ga-As bonds near the (110) surface of ZB crystal, in agreement with QM results (see Fig. S1 in the supplementary material[9]).

The bond contraction near the $\{1\bar{1}0\}$ sidewalls leads to a core/shell structure of the NW. To show this, the NW is relaxed to the minimum energy configuration with the periodic boundary condition (PBC) applied only to the [111] axial direction. Figures 1(b) and 1(c) show the core/shell structure with three-fold symmetry. Figure 1(b) is the top view of the atomic bond structure of the NW, where bonds are color-coded according to the bond length. In particular, three of the six corners have the shortest bonds (colored in black), while the bond lengths at the other 3 corners (green) are slightly larger but still shorter than the bulk crystalline value. All bonds along the edge (blue) have the length between the two contracted corner bond lengths. In contrast to these contracted bonds in the shell, all bonds in the inner core of the NW (red) have the same length as the bulk crystalline bonds, while some bonds in the transient region between the shell and the core (yellow) are longer than the bulk bond. Figure 1(c) is the top view of slip-vector field of the same NW. As described in Ref. 9, the slip vector quantifies the displacement of atoms relative to their neighbors in the reference system (i.e., a system without relaxation) and contains information about the slip plane and Burgers vector.[11] From the slip-vector field and the bond-network structure, we can see that the outermost layer of atoms moves towards the inner core of the NW as a result of the bond contraction. At the same time, the atomic bonds in the next layer, which moves outward with less magnitude, are stretched. Similar to the two outermost layers, the third atomic layer moves towards the inner core due to bond contraction, while the next layer moves outwards. From Figs. 1(b) and 1(c), the shell depth is estimated to be 7 atomic layers from the edge. For the 30 Å NW, the shell/core volume ratio is as large as 4/1. The [111]-oriented ZB NW is a stack of three types of GaAs bilayers, and each bilayer exhibits a distinct three-fold symmetry (Fig. S2).[9] This is in contrast to a similar core/shell structure found in a [0001]-oriented wurtzite crystalline NW, where all bilayers have the identical six-fold symmetry.[12]

The core/shell structure in Fig. 1 has a significant effect on the adsorption energy of Ga and As atoms on the top surface of the NW. To quantify this effect, we remove the axial PBC to relax the top (111)B free surface of the [111]-oriented NW. We then calculate the energy of a Ga adatom at all possible adsorptions sites on the top surface (Fig. 2(a)). Note that the GaAs (111)B surface is As terminated, and Ga atoms need to be deposited first on top of the topmost As

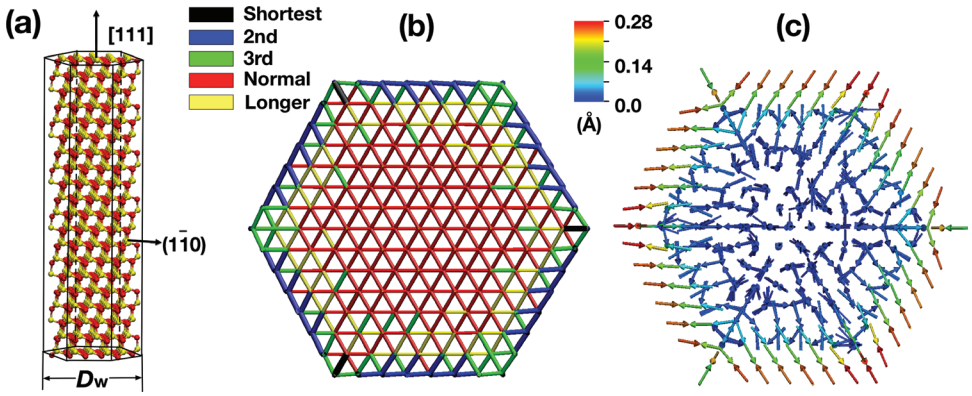

FIG. 1. (a) Schematic of the simulated GaAs NW. (b) Top view of the atomic bond structure in the NW, where bonds are colored according to the bond length. (c) Top view of the color-coded slip-vector field.

atoms for subsequent layers to grow. Figures 2(b) and 2(c) show the Ga adatom energy along the blue and red lines marked in Fig. 2(a), which respectively include the corner and edge sites at the ends. Figure 2(b) shows the lowest energies for the two NW corners (i.e., the left and right ends of the blue line in Fig. 2(a)), but the two corners are not equivalent because of the three-fold symmetry explained before. Figure 2(c) shows that the edges of the NW (i.e., the left and right ends of the red line in Fig. 2(a)) also have lower energies than the core of the NW. Figure 2(d) shows the spatial distribution of the adatom energy on the entire NW top. The adatom energy map reflects the core/shell structure in Fig. 1. Namely, the adatom energies are lower in the shell compared with those in the core. In particular, three corners of the top surface have the lowest adsorption energy. This result suggests that atoms are adsorbed preferentially at the corners and edges of the NW top surface.

Based on the above observation, we construct a simple nucleation growth model,[8] in which an island of a GaAs bilayer is nucleated at a corner of the NW top surface (Fig. 3(a)). For simplicity, we choose a hexagonal island consisting of N adatoms. Here, the Ga atoms are placed on top of As atoms on the NW top surface, whereas the placement of the As atoms is at either ZB (Fig. S2(a)) or fault (Fig. S2(b)) sites.[9] The [111]-oriented ZB crystalline GaAs NW is a stack of alternating Ga and As monolayers (MLs), where each ML is a two-dimensional triangular lattice of either Ga or As atoms. According to the lateral positions occupied by the atoms, the triangular lattices are classified into three types: "A," "B," and "C." Let the stacking sequence of the top three As MLs be ABC, where C is the topmost ML. Then, the deposited bilayer consists of a Ga ML in the C triangular lattice and an As ML in two possible triangular lattices. Namely, As adatoms in a ZB island occupy the A triangular lattice, i.e. (···ABC)A stacking, whereas As atoms in a fault island occupy the B triangular lattice, (···ABC)B. The fault stacking in the latter is common to all stacking defects, including twins as well as intrinsic and extrinsic SFs.[13]

Figure 3(b) shows the energy per adatom, $E(N)/N$, for ZB and fault islands as a function of N. The core/shell structure shown in Figs. 1 and 2 is reflected here in the lower fault island energy than the ZB island energy for small N. Figure 3(b) also shows the asymptotic energies for $N \to \infty$ (i.e., infinite ad-bilayer) by arrows, where the fault energy is higher than the ZB energy by 7.8 meV per atom. These asymptotic energies have been computed for a slab with (111) free

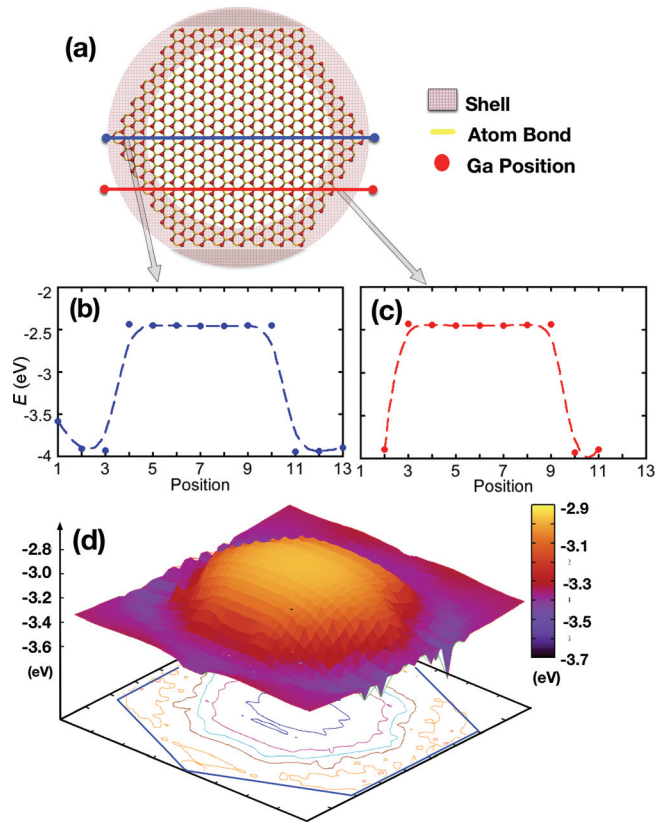

FIG. 2. (a) Schematic of the calculation of ad-atom energy map, where red circles and yellow lines represent Ga adsorption sites and Ga-As bonds in the top bilayer, respectively. The shell region is shaded in magenta. (b) and (c) Ga adatom energy along the blue and red lines marked in (a), respectively. (d) The adatom energy map of the entire NW top surface.

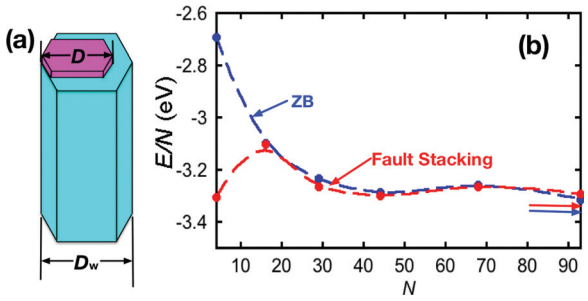

FIG. 3. (a) Schematic of a GaAs bilayer island (magenta) nucleated at a corner of the top surface of a NW (cyan). (b) ZB (blue) and fault (red) island energies per atom as a function of the number of adatoms. The asymptotic limit of the ZB and fault energies are indicated by the blue and red arrows, respectively.

surfaces with PBCs in the lateral directions, where either a ZB (Fig. S2(a)) or fault (Fig. S2(b)) bilayer is deposited on top of the (111)B top surface of the slab.[9] The most important consequence of the adatom core/shell structure here is a crossover of the island size ($N \sim 70$), above which ZB islands become energetically more stable than fault islands. Namely, small adatom islands nucleated at NW corners are likely to occupy fault stacking sites, whereas larger islands energetically favor regular ZB stacking.

The crossover of the island energetics in Fig. 3 has major consequences on the NW growth. To show this, we calculate the change of Gibbs free energy due to the nucleation of an island[14,15] in the presence of reactant vapor by subtracting the free energy of the gas from the island energy as $G = E - N_{\mathrm{Ga}}\mu_{\mathrm{Ga}}^{\mathrm{gas}} - N_{\mathrm{As}}\mu_{\mathrm{As}}^{\mathrm{gas}}$. Here, $\mu_{\mathrm{Ga}}^{\mathrm{gas}}$ and $\mu_{\mathrm{As}}^{\mathrm{gas}}$ are the gas-phase chemical potentials of Ga and As, which depend on the growth temperature and the partial vapor pressures, P_{Ga} and P_{As}, of Ga and As, and N_{Ga} and N_{As} are the numbers of Ga and As atoms.[9] Figure 4(a) shows G as a function of the island diameter D at two temperatures, $T = 1030$ and 1050 K, where $P_{\mathrm{Ga}} = 2.7 \times 10^{-6}$ bar and $P_{\mathrm{As}} = 5.0 \times 10^{-4}$ bar.[14] These temperatures are within the optimal growth temperature window that is sufficiently high for detrimental surface As-trimers to be desorbed but is low enough not to cause the desorption of adatoms.[6] The critical nucleus size D^* and the activation barrier $G^* = G(D^*)$ for growth are obtained by the peak position and height of each curve, respectively (indicated by the arrows in Fig. 4(a)). At the lower temperature, the fault island has the lower G^* (see the red solid line) than the ZB island (see the blue solid line) and is likely to grow. At the higher temperature, in contrast, the ZB island (see the blue dashed line) is likely to grow.

We calculate the critical nucleus sizes of ZB and fault islands at different temperatures. The result in Fig. 4(b) exhibits a crossover phenomenon: At lower temperatures, fault islands have smaller critical diameters than ZB islands, $D^*_{\mathrm{fault}} < D^*_{\mathrm{ZB}}$, while at higher temperatures, $D^*_{\mathrm{ZB}} < D^*_{\mathrm{fault}}$. The probability of fault-layer generation is calculated as $p_{\mathrm{fault}} = \exp(-G^*_{\mathrm{fault}}/k_{\mathrm{B}}T)/[\exp(-G^*_{\mathrm{fault}}/k_{\mathrm{B}}T) + \exp(-G^*_{\mathrm{ZB}}/k_{\mathrm{B}}T)]$, where k_{B} is the Boltzmann constant.[16] In general, the larger the critical nucleus, the larger the activation barrier, and hence the slower is the growth rate. Figure 4(b) indicates that fewer SFs are generated under such conditions. This analysis shows that the growth temperature and partial pressures can be controlled to minimize SFs. In addition to the growth temperature and pressure control of SF density, Fig. 4(b) suggests a size-controlled growth method for completely eliminating SFs. Namely, if the diameter D_{W} of the NW is between the critical nucleus sizes of ZB and fault islands, i.e., $D^*_{\mathrm{ZB}} < D_{\mathrm{W}} < D^*_{\mathrm{fault}}$, only ZB islands but no fault islands can grow on the NW top surface. The SF-free growth range is indicated by the yellow area in Fig. 4(b). Our simulation results thus suggest a possibility of SA-MOVPE growth of SF-free NWs with judicious choice of diameter, growth temperature, and vapor pressures.[17]

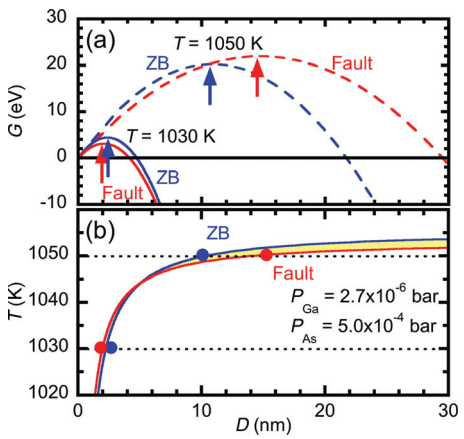

FIG. 4. (a) Gibbs free-energy changes of ZB (blue) and fault (red) islands of a Ga-As bilayer adsorbed on the GaAs NW as a function of the island diameter at temperature $T = 1030$ K (solid lines) and 1050 K (dashed lines). The peak position (i.e., the critical nucleus size) of each curve is indicated by an arrow. (b) Critical nucleus sizes of ZB (blue) and fault (red) islands as a function of the temperature. The yellow area indicates (D_{W}, T) pairs, for which NWs are grown free of SF. The vapor pressures are $P_{\mathrm{Ga}} = 2.7 \times 10^{-6}$ bar and $P_{\mathrm{As}} = 5 \times 10^{-4}$ bar.

In summary, MD simulation has revealed a core/shell structure for the adatom energetics on the (111)B top surface of a [111]-oriented GaAs NW, in which SFs are preferentially nucleated in the shell. Based on this atomistic understanding, we have proposed size-controlled growth of SF-free NWs.

This work was supported by the U.S. Department of Energy, Office of Science, Office of Basic Energy Sciences under Award DE-SC0001013 as part of the Center for Energy Nanoscience, an Energy Frontier Research Center. Simulations were performed at the University of Southern California using the 20,925-processor Linux cluster at the High Performance Computing Facility. We thank Daniel Dapkus, Chun-Yung Chi, Shu Hu, and Maoqing Yao for useful discussions.

[1]J. A. Czaban, D. A. Thompson, and R. R. LaPierre, Nano Lett. **9**(1), 148–154 (2009).
[2]T. Zhu and J. Li, Prog. Mater. Sci. **55**(7), 710–757 (2010).
[3]J. R. Greer and J. T. M. De Hosson, Prog. Mater. Sci. **56**(6), 654–724 (2011).
[4]Y. B. Wang, H. J. Joyce, Q. A. Gao, X. Z. Liao, H. H. Tan, J. Zou, S. P. Ringer, Z. W. Shan, and C. Jagadish, Nano Lett. **11**(4), 1546–1549 (2011).
[5]A. I. Persson, M. W. Larsson, S. Stenstrom, B. J. Ohlsson, L. Samuelson, and L. R. Wallenberg, Nat. Mater. **3**(10), 677–681 (2004).
[6]K. Tomioka, K. Ikejiri, T. Tanaka, J. Motohisa, S. Hara, K. Hiruma, and T. Fukui, J. Mater. Res. **26**(17), 2127–2141 (2011).
[7]D. Rudolph, S. Hertenberger, S. Bolte, W. Paosangthong, D. Spirkoska, M. Doblinger, M. Bichler, J. J. Finley, G. Abstreiter, and G. Koblmuller, Nano Lett. **11**(9), 3848–3854 (2011).
[8]F. Glas, J. C. Harmand, and G. Patriarche, Phys. Rev. Lett. **99**(14), 146101 (2007).
[9]See supplementary material at http://dx.doi.org/10.1063/1.3703765 for simulation details.
[10]S. Kodiyalam, R. K. Kalia, A. Nakano, and P. Vashishta, Phys. Rev. Lett. **93**(20), 203401 (2004).
[11]J. A. Zimmerman, C. L. Kelchner, P. A. Klein, J. C. Hamilton, and S. M. Foiles, Phys. Rev. Lett. **87**(16), 165507 (2001).
[12]Z. Yuan, K. Nomura, and A. Nakano, Appl. Phys. Lett. "*Core/shell structural transformation and brittle-to-ductile transition in nanowires*," Appl. Phys. Lett. (to be published).
[13]F. Glas, J. Appl. Phys. **104**(9), 093520 (2008).
[14]K. Ikejiri, T. Sato, H. Yoshida, K. Hiruma, J. Motohisa, S. Hara, and T. Fukui, Nanotechnology **19**(26), 265504 (2008).
[15]J. Johansson, L. S. Karlsson, C. P. T. Svensson, T. Martensson, B. A. Wacaser, K. Deppert, L. Samuelson, and W. Seifert, Nat. Mater. **5**(7), 574–580 (2006).
[16]J. Johansson, L. S. Karlsson, K. A. Dick, J. Bolinsson, B. A. Wacaser, K. Deppert, and L. Samuelson, Cryst. Growth Design **9**(2), 766–773 (2009).
[17]We should note that the Gibbs free energy here is based on a simple ideal gas model, and more realistic estimate should include reaction chemistry, which is beyond the scope of this paper. See, e.g., T. R. Omstead and K. F. Jensen, Chem. Mater. **2**(1), 39–49 (1990).